Mixing and deformations in mantle plumes

Cinzia G. Farnetani [a,*], Bernard Legras [b], Paul J. Tackley [c]

[a] *Institut de Physique du Globe de Paris, Laboratoire de Dynamique des Systemes Geologiques, Boite 89, 4, place Jussieu, 75252 Paris Cedex 05, France*
[b] *Ecole Normale Supérieure, Paris, France*
[c] *University of California, Los Angeles, CA, USA*

Abstract

The long standing idea that the source of oceanic island basalts includes ancient subducted material is strengthened by recent geochemical observations for Hawaii [Lassiter and Hauri, Earth Planet. Sci. Lett. 164 (1998) 483−496] and Iceland [Kempton et al., Earth Planet. Sci. Lett. 177 (2000) 255−271]. In particular, the isotopic variations in Hawaiian shield lavas indicate the presence of two distinct recycled components: ancient oceanic crust+sediments, and altered ultramafic lower crust or lithospheric mantle. Lassiter and Hauri [Earth Planet. Sci. Lett. 164 (1998) 483−496] suggest that both components are from the same packet of recycled oceanic lithosphere, thus implying that chemical heterogeneities a few km thick can be preserved in the convecting mantle. In this paper we investigate the role of mantle plumes in stirring mantle heterogeneities and we address the following questions: (1) Is the heterogeneous nature of plumes inherited at the source or does it develop through entrainment? (2) Is stirring more efficient in the plume head or in the long-lived plume tail? (3) Are the geochemical implications consistent with fluid dynamical models? We use a three-dimensional numerical model in Cartesian geometry to simulate the dynamics of an isolated plume. Transport calculations, conducted on a vertical plane of symmetry, allow us to advect passive tracers forward or backward in time to investigate mixing. We also calculate the finite-time Lyapunov exponents in order to quantify the deformations associated to the plume rise. Our results show that: (1) the thermal boundary layer, where the plume forms, is the region most efficiently sampled by a mantle plume. Since the overlying mantle is not entrained in the plume head, we speculate that the geochemically heterogeneous nature of plumes is inherited from the source. Our results also predict the absence of present-day upper mantle, source of MORB, in plume lavas. (2) Heterogeneities initially located in the source region undergo a series of stretching and folding events while rising in the plume head and may be reduced to narrow filaments. We find that stirring is more important in the plume head than in the long-lived plume tail. Therefore, our results predict that distinct geochemical heterogeneities are more likely to be found in hotspot lavas rather than in flood basalt lavas, associated to partial melting of a plume tail and a plume head [Richards et al., Science 246 (1989) 103–107], respectively. (3) High Lyapunov exponents, indicating high deformations, are found at the frontier between the plume head and the sublithospheric mantle surrounding the plume head. We speculate that the arrival of a large plume head could induce seismic anisotropy in the shallow upper mantle. © 2002 Elsevier Science B.V. All rights reserved.

---

* Corresponding author. Tel: +33-1-4427-4796; Fax: +33-1-4427-2481.   *E-mail address:* cinzia@ipgp.jussieu.fr (C.G. Farnetani).

1. Introduction

Geochemical analysis on lavas from Hawaii and Iceland, the most vigorous present-day hotspots, provide compelling evidences on the heterogeneous nature of mantle plumes. A plume probably consists of a mixture of enriched and more fusible streaks in a depleted and refractory matrix. The depleted component in plumes seems to be different from the depleted upper mantle source of MORBs. According to Kempton et al. [2] the depleted component present in the Iceland plume differs from the depleted upper mantle sampled by the present-day North Atlantic mid-ocean ridge. The high hafnium isotope ratio of the depleted component is a long-lived and intrinsic feature of the Iceland plume and is probably generated by ancient melting events. Moreover a long term isolation of the different components is necessary to generate the isotope ratios observed in Icelandic basalts. Similarly, for Hawaii, the depleted upper mantle component is very minor or non-existent [4]. This is in agreement with oxygen–osmium–lead isotope correlations by Lassiter and Hauri [1] precluding the generation of the Kea isotopic signature from astenospheric upper mantle. It is also in agreement with the lead–hafnium isotopic relations [5] indicating that upper mantle material is not involved in the production of the Hawaiian basalts.

The enriched component in plumes is most likely associated to the presence of recycled oceanic crust, as first suggested by Hofmann and White [6]. Recently Lassiter and Hauri [1] have used oxygen–osmium–lead isotopes to constrain the nature of the plume material feeding the Koolau and the Kea trends in Hawaii. They find that the radiogenic Os isotopes and anomalously heavy oxygen isotopes for the Koolau lavas reflect melt generation from recycled oceanic crust plus pelagic sediment, while for the Kea lavas the unradiogenic Os isotopes and anomalously light oxygen isotopes reflect the presence of recycled, hydrothermally altered, ultramafic lower crust or lithospheric mantle. The presence of old pelagic sediments in the source of Koolau component has also been identified by Blichert-Toft et al. [5], using hafnium isotopic data.

Therefore, the most recent geochemical studies on lavas from Iceland and Hawaii seem to indicate that the most important geochemical components in a mantle plume are both related to the same dynamical process: the subduction of the oceanic lithosphere with crust and sediments, their storage in the Earth's mantle for at least 1 billion years, their incorporation in mantle plumes. For vigorous mantle plumes, such as Iceland and Hawaii, one more component may be present: a small fraction of relatively undegassed material that could explain the helium and neon isotopic ratios. The high $^3He/^4He$ ratio for Hawaii and for Iceland has been generally attributed to the presence of an 'undegassed' reservoir, rich in primitive ^3He. Also the identification of near-solar neon isotopic ratios in some glasses from Loihi and Kilauea [7] and from Iceland [8,9] suggests the presence of an 'undegassed' mantle component with high $[Ne_{solar}]/[U+Th]$.

In mantle plumes there are therefore at least three distinct components and the understanding of their origin and evolution may provide major constraints on the style of mantle convection, on the efficiency of mixing in the Earth's interior, and on the fluid dynamics of plumes.

A first important geodynamic implication concerns the fate of subducted material. Seismic tomography (e.g., [10] and references therein) shows that slab penetrate in the lower mantle in spite of the inhibiting effect of the phase transition at 660 km depth. However, one can speculate that the style of mantle convection changed over time and that convection in the past was predominantly layered [11]. The age of the recycled material in mantle plumes could represent a key parameter to test this hypothesis: if the subducted lithosphere remained isolated for 1 Ga, or may be up to 3 Ga (the age of the sediments estimated by [5]) then the subducted material was more likely stored in the lower mantle, rather than in the upper mantle continuously sampled by spreading ridges. This would support the idea that whole mantle convection was active also in the past.

A second important geodynamic implication concerns the efficiency of mixing of the subducted material. According to Lassiter and Hauri [1] the preservation of both upper- and lower-crustal

oxygen isotope signatures in Hawaiian lavas, indicates that chemical heterogeneities with length scales of only a few kilometers can be preserved in the convecting mantle for long periods of time. Similarly, Sobolev at al. [12] working on 'ghost plagioclase' trace-element signature in inclusions in Mauna Loa olivines, infer that subducted and recycled crustal gabbro can retain much of its original chemical identity through the convective cycle. These observations support the idea that the subducted crust does not mix completely with the peridotitic matrix, but remains distinct forming a 'marble cake' mantle, as first suggested by Allègre and Turcotte [13]. We also note that due to the negligible rate of chemical diffusion any compositional difference in the mantle is only stirred, not mixed.

The third important geodynamic implication concerns the preservation of more undegassed material in a convecting mantle [14] and the existence of two distinct OIB and MORB sources.

In order to understand the geochemical message brought to the surface by plumes we need to address some fundamental questions such as 'Which regions of the mantle are more efficiently sampled by mantle plumes?' and 'Is the heterogeneous nature of mantle plumes inherited at the source or does it develop through entrainment of various components during the ascent to the surface?' In this paper we use a three-dimensional numerical model in Cartesian geometry to solve for the solid-state dynamics of an isolated mantle plume from the lower mantle. Passive heterogeneities are modeled by tracers that can be advected forward in time as well as backward in time. We also calculate the finite-time deformations induced by the rise of a plume, thus enabling us to address another question: 'Where does most of the deformation take place when a plume rises: within the plume or in the surrounding mantle?'

Our conceptual model is designed to study the dynamics of a strong plume, such as Iceland or Hawaii for which there is ample geochemical and geophysical evidence that they originate in the lower mantle. In the models we vary the mantle viscosity structure and we can include the dynamic effect of the endothermic phase transition at 660 km depth.

We find that the region most efficiently sampled is the thermal boundary layer where the plume originates, while the surrounding mantle, through which the plume rises, is very poorly sampled. Our results, showing negligible entrainment in mantle plumes are consistent with previous numerical models [15], while they disagree with early laboratory experiments [16]. The most important reason is the different initial condition for plume formation: instability at a thermal boundary, versus injection of hot fluid from a point source. We find that the upper mantle material is not entrained in the plume head, rather it is displaced by the plume and forms a sheath surrounding the hot plume. Therefore, our results predict the absence of any geochemical signature of present-day upper mantle in plume lavas. By calculating the Lyapunov exponents we quantify the deformations and we find that mantle material forming the plume head is more deformed (by a series of stretching and folding events) than the material in the plume tail, that undergoes mainly stretching.

2. Numerical model

We use the Cartesian three-dimensional numerical model STAG3D by Paul Tackley. The model simulates the dynamics of solid-state convection by solving the equations for the conservation of mass, conservation of momentum, and conservation of energy for a viscous fluid at infinite Prandtl number. It also solves the advection equation of an active chemical field which allows us to investigate the role of chemically denser material at the base of the mantle. The slight numerical diffusion that arises when advecting sharp interfaces is corrected by applying the filter of [17]. It is out of the purpose of this paper to describe in detail the model which has been thoroughly presented elsewhere, (e.g., [18] and references therein).

The size of our domain in the x, y, and z directions is $2900 \times 1450 \times 2900$ km, respectively, meshed by $128 \times 64 \times 128$ elements. Hence, the element size is 22.6 km/element in the horizontal directions, while it is 15 km/element in the vertical

direction for the bottom 300 km, and 24 km/element above.

The physical parameters used to normalize the equations are: the mantle depth $D = 2900$ km, the potential temperature contrast between the surface and the bottom $\Delta\theta = 1800°C$, the mantle density $\rho = 4000$ kg m^{-3}, which is constant by the Boussinesq approximation, the thermal expansion coefficient $\alpha = 2 \times 10^{-5}$ K^{-1}, the thermal diffusivity $\kappa = 10^{-6}$ m^{2}s^{-1}, the reference mantle viscosity $\eta_m = 10^{22}$ Pa s for $\theta_m = 1300°C$. Using the above values the Rayleigh number is 3.5×10^6.

The viscosity is temperature-dependent according to the exponential law:

$$\eta(\theta) = \eta_m \exp[23(\theta_m - \theta)] \qquad (1)$$

which gives a min $\eta_{plume} = 0.01 \; \eta_m$ and max $\eta_{lithosphere} = 30 \; \eta_m$, where η_m is the viscosity of the surrounding mantle. We also explore stratified models with viscosity ratio between upper and lower mantle $\eta_{UM}/\eta_{LM} = 1/30$.

The velocity boundary conditions are free slip for the top and the bottom and no incoming or outgoing flux is allowed through the walls. For the vertical wall xz (at $y = 0$) we use reflecting boundary conditions since we only model half of the plume. In fact the plume is centered in the middle of the x-axis (at $x = 1450$ km) and at $y = 0$. We remark that although our calculations are conducted in three dimensions, all the results presented in this paper are relative to an axisymmetric case. The boundary conditions for the potential temperature field are constant at the surface ($\theta = 0°C$) and at the bottom ($\theta = 1800°C$), while the vertical walls are insulated. At the initial time, the potential temperature is constant throughout the mantle ($\theta = 1300°C$), while there is a thermal boundary layer 120 km thick at the bottom, where the temperature profile increases across as an error function. In order to trigger the plume formation we apply a small perturbation (max is 1% $\Delta\theta$) which decreases linearly with radial distance. Because of this initial setting, the motion stays essentially axisymmetric during the whole simulation period.

All the boundaries are impermeable to the chemical field. The initial value of the chemical field is zero everywhere, except for a layer 20 km thick at the bottom of the mantle. This thin layer has a chemical excess density of 2% with respect to the surrounding mantle ($\Delta\rho_{ch}/\Delta\rho_{th} = 0.55$). We use the active chemical field only for one model since it is out of the purpose of this paper to vary systematically the thickness and the excess density of the chemically denser layer. Our choice of a 20-km thick layer corresponds to an average thickness of the ultra low velocity layer detected at the base of the Earth's mantle [19], which has a variable thickness between 0 and 40 km. For a more extensive investigation of the role of chemical stratification across D″ on mantle plume dynamics see [20].

2.1. Transport calculations

The advection of passive tracers is performed off-line from the archived velocity field of the model. Because of the axisymmetric symmetry we only use velocity components in the vertical y–z plane at $x = 1450$ km saved at each time step. The advection is performed using a two-dimensional bicubic spline interpolation within the mesh of the model [21] and using a second-order Runge–Kutta method for the time scheme. More than half a million trajectories are calculated forward and backward in time.

The forward integration starts at the initial time t_0. It is particularly interesting to put the tracers within a few hundred km above the core mantle boundary. The backward integration starts at the final time t_1 when the plume head has spread beneath the lithosphere. Tracers are distributed regularly in each grid element and by advecting them backward to the initial time we can understand where each tracer comes from.

We calculate the deformation associated with the rise of the plume, represented by the finite-time Lyapunov exponents. The Lyapunov exponents are a convenient indicator of the sensitivity to small perturbations of the initial position and provide the exponential rate of divergence of infinitesimally nearby initial trajectories. By integrating the deformation along each tracer trajectory we can understand (i) where is initially located the material which deforms the most dur-

ing the formation and the ascent of the plume and (ii) where is located this highly deformed material when the plume head arrives beneath the lithosphere.

To calculate the finite-time Lyapunov exponents we consider a trajectory x, starting at the position x_0 at time t_0 and ending at the position x_1 at time t_1. The velocity vector at each position x along the trajectory and time t is given by:

$$\frac{\mathrm{d}x}{\mathrm{d}t} = u(x, t) \qquad (2)$$

The infinitesimal displacement ξ_0 at time t_0 is transformed into ξ_1 at time t_1 by:

$$\xi_1 = M(x_0, t_0; x_1, t_1)\xi_0, \qquad (3)$$

where M is a linear operator given by the integration of:

$$\frac{\mathrm{d}M}{\mathrm{d}t} = \frac{Du}{Dx}M \qquad (4)$$

along the trajectory, where Du/Dx is the material derivative of the velocity. At the initial time t_0 the matrix M corresponds to the identity matrix:

$$M(x_0, t_0; x_0, t_0) = \text{Identity} \qquad (5)$$

The variation of the displacement over the interval $[t_0, t_1]$ is given by the ratio:

$$\frac{|\xi|}{|\xi_0|} = \frac{|M\xi_0|}{|\xi_0|} = \left(\frac{\xi_0^T M^T M \xi_0}{\xi_0^T \xi_0}\right)^{1/2}$$

This ratio is governed by the real eigenvalues σ_+ and σ_- of $M^T M$, the right Cauchy–Green strain tensor [22], and the projection of ξ_0 onto its eigenvectors. The finite-time Lyapunov exponents or finite-time deformations are defined as:

$$\lambda_+ = \frac{1}{t_1 - t_0}\ln \sigma_+ \qquad (6)$$

$$\lambda_- = \frac{1}{t_1 - t_0}\ln \sigma_-$$

They are calculated by numerical integration of Eq. 4 for the discretized version of Du/Dx along

the particle trajectory. See [23] for a detailed discussion.

A circular blob of tracers with unit radius surrounding x_0 at time t_0 is turned into an ellipsoid surrounding x_1 at time t_1 with semi-axis of length σ_+ and σ_-. Conversely a circular blob of tracers with unit radius surrounding x_1 at time t_1 was an ellipsoid with axis $1/\sigma_+$ and $1/\sigma_-$ surrounding x_0 at time t_0. Because the motion preserves volume in three dimensions:

$$\lambda_+ + \lambda_- = \frac{1}{t_1 - t_0}\ln \frac{r_0}{r_1} \qquad (7)$$

where r_0 and r_1 are the initial and the final radial distances.

Because of the exponential separation of σ_+ and σ_-, the eigenvalue problem is badly conditioned for M and, in practice, only λ_+ can be obtained with some accuracy in forward integration. Since M is transformed into M^{-1} by reversing time, λ_- can be obtained by backward integration.

3. Results

3.1. Plume dynamics and tracers advection

The simplest model, thereafter called Model 1, has a uniform background mantle viscosity $\eta_m = 10^{22}$ Pa s and varying η_{plume} which can be as small as $0.01\eta_m$. Fig. 1a shows the initial condition for the temperature field on the y–z plane at $x = 1450$ km, colors indicate the excess temperature with respect to the mantle. Fig. 1b shows the initial position of the passive tracers, each 'pack' of tracers is 100 km high and 180 km long. The plume head radius is 250 km wide (Fig. 1c) at the elapsed time $t_e = 105$ Myr (notice that a long time of ca. 80–90 Myr, elapses from the initial condition to the stage when a very small plume forms). Fig. 1d shows that tracers initially close to the axis form a stretched boundary of the plume head, while tracers that are as far as 1000 km are stretched and travel rapidly at the bottom of the thermal boundary layer where the horizontal velocities are important. At $t_e = 135$
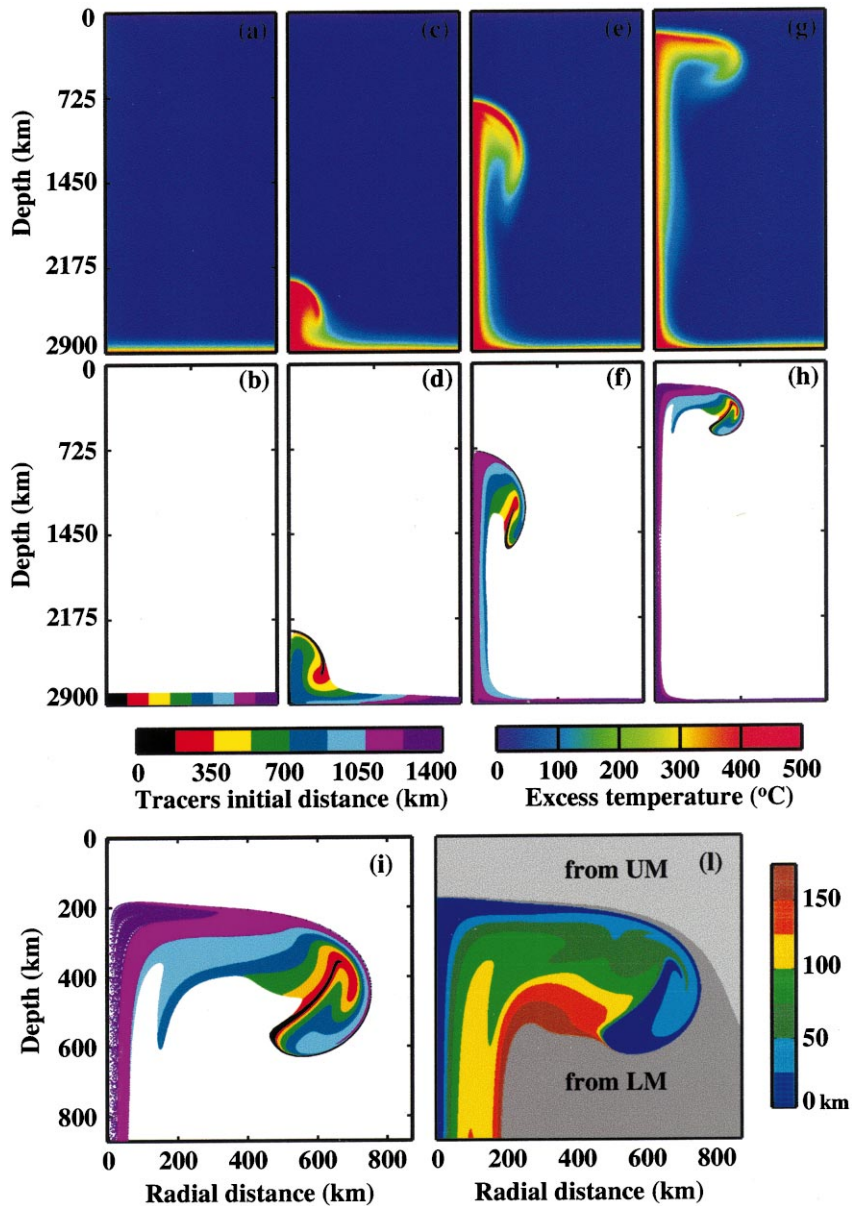
Fig. 1. Plume evolution for Model 1. Top: excess temperature, (a) initial condition, (c,e) later stages, (g) final stage. Middle: tracers advected forward, (b) initial condition, (d,f,h) later stages. (i) Detail of the plume head shown in 1h. (l) Tracers advected backward. Color scale indicates the height above the CMB (see text).

Myr the plume is at 800 km depth, its radius is 380 km and there is no evidence of efficient entrainment within the plume head (Fig. 1e). The tracers initially up to 700 km far from the axis (Fig. 1f) are in a torus within the plume head that has been stretched and folded. This torus rises more slowly than material closer to the axis. Tracers in the axial part of the plume come from a great radial distance and rise very rapidly in the plume conduit. Fig. 1g shows a large plume head, 650 km radius, spread beneath the lithosphere at $t_e = 175$ Myr. The correspond-

ing tracers position (Fig. 1h) indicates that all the material in the plume head comes from the thermal boundary layer. Material in the tail has been stretched, while material in the head has been stretched and folded. A detail of the plume head for this final step is shown in Fig. 1i. The plume head is heterogeneous since tracers with different initial position get close by in the plume head. The results of the backward calculation are shown in Fig. 1l. Colors now correspond to the calculated depth of origin of each tracer. Tracers with calculated initial position in the upper mantle are in light gray, tracers that come from the lower mantle are in dark gray, while tracers coming from the bottom of the mantle are shown with rainbow colors. The good agreement between the the shape of the head Fig. 1i,l is an indicator of the accuracy of the numerical integration. Since the tracers are put on a regular grid at t_1, Fig. 1l is plotted with a uniform spatial resolution while the dispersion of tracers in Fig. 1i reduces the resolution in the plume core. A clear result is that upper mantle material is pushed away by the rising plume head and does not enter in the plume head. By comparing Fig. 1i,l, it is apparent that the tail is formed by concentric cylinders originating from sloping surfaces across the D″ layer and that the motion is more efficient at stirring lateral inhomogeneities than vertical inhomogeneities.

In Model 2 the mantle is stratified with a viscosity jump at 660 km. The viscosity ratio between the upper mantle and the lower mantle $\eta_{UM}/\eta_{LM} = 1/30$ and, as above, min $\eta_{plume} \approx 0.01\eta_m$. The excess temperature (Fig. 2a) and the tracers position (Fig. 2b) when the plume head is at 1700 km depth (at $t_e = 115$ Myr) are similar to the previous model since the conditions in the lower mantle are unchanged. Fig. 2c shows the plume at 660 km depth at $t_e = 130$ Myr. The part of the plume closer to the axis ascends rapidly in the upper mantle, while the part of the head still in the lower mantle rises more slowly. The effect of the viscosity jump at 660 km depth profoundly affects the shape of the head and the degree of stretching of the rising material. At $t_e = 132$ Myr a relatively small plume head (radius = 300 km) reaches the base of the

lithosphere, while a long stretch of hot material remains in the lower mantle (Fig. 2e). The head is composed of tracers that were originally at more than 1000 km from the axis (Fig. 2f), while material initially closer to the axis constitutes the long stretch still in the lower mantle. After 139 Myr the plume head has spread beneath the lithosphere (Fig. 2g), its excess temperature is complex: a hot part ($\Delta\theta = 350$–$400°C$) surrounds a colder central part ($\Delta\theta = 100°C$). The hot part corresponds to the location of the tracers from the lowermost 100 km (Fig. 2h). It is also evident that some tracers 'packs' are reduced to narrow filaments and the deformation is considerable. A detail of the plume head is shown in Fig. 2i, the different colors indicate that the head is heterogeneous, mainly in the distal part of the plume head. The results of the backward calculation indicate that the colder central part of the plume head is made of material coming from 100–150 km above the CMB (Fig. 2l). Compared to the previous model, the viscosity jump at 660 km depth has the effect of reducing the volume of the plume head, increasing stirring of the deep mantle material that constitutes the head, while the entrainment of upper mantle in the head is absent in both models.

For Model 3 a thin and chemically denser layer is present at the base of the mantle, while the mantle viscosity is identical to Model 2. The presence of chemical heterogeneities significantly affects the dynamics and the final structure and composition of a plume. Since the hottest part of the thermal boundary layer remains at the bottom, the excess temperature of the plume is reduced to $\Delta\theta = 200$–$300°C$ and it is more realistic than in the previous models. The colder temperature induces a weaker viscosity contrast between the plume and the surrounding mantle, therefore the shape of the plume is now more similar to a 'spout' than to a 'mushroom' (Fig. 3a). Fig. 3b shows that part of the tracers pile up at the bottom and form a large 'foot', while the head is composed of stretched deep material. The presence of a 'foot' facilitates the rise of tracers initially at more than 1000 km from the axis (Fig. 3d,f). The plume head narrows while entering in the low viscosity upper mantle (Fig. 3e) further
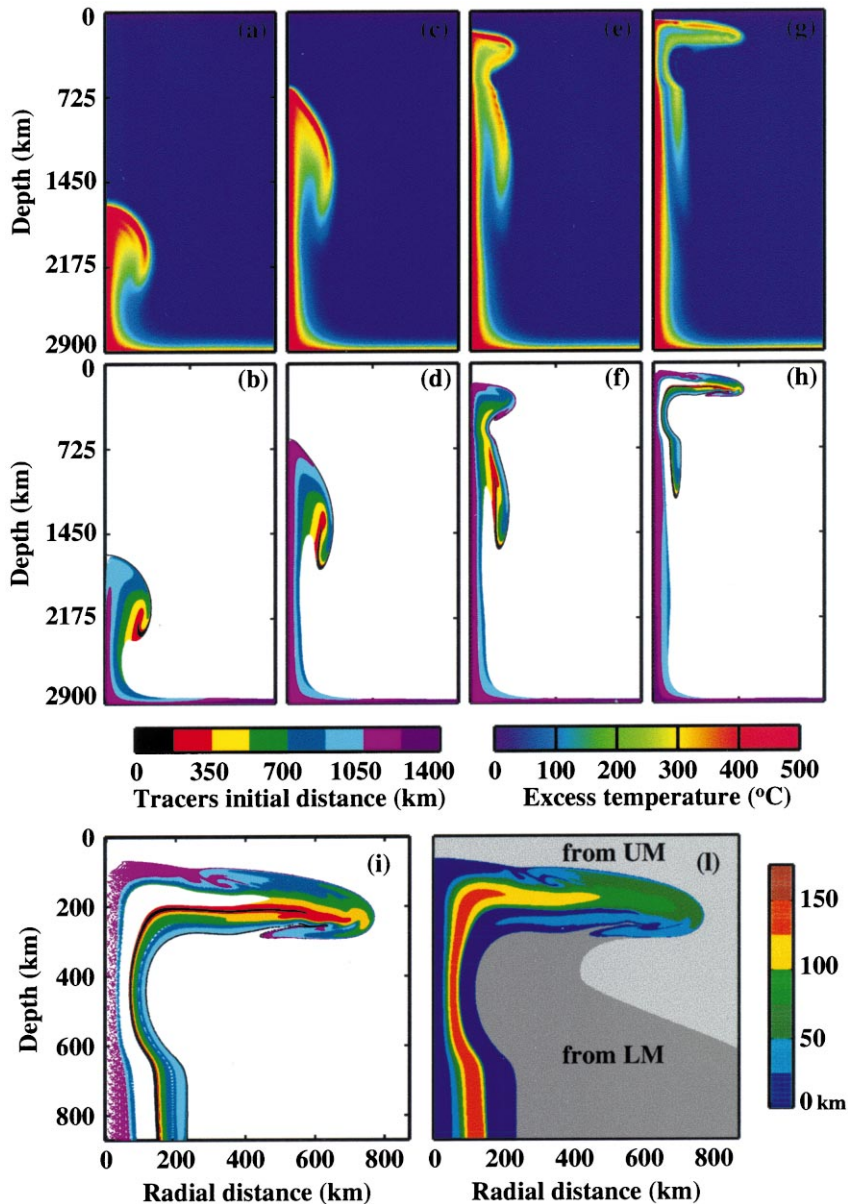
Fig. 2. Plume evolution for Model 2. Top: excess temperature. Middle: tracers advected forward. (i) Detail of the plume head shown in 2h. (l) Tracers advected backward.

stretching the ascending material (Fig. 3f). The plume head spreading beneath the lithosphere is shown in Fig. 3g at the elapsed time $t_e = 290$ Myr. This long elapsed time is due to the presence of denser material in the thermal boundary layer which hinders plume formation: nearly 200 Myr are necessary to form a small initial plume which

then ascends in ca. 90 Myr. The tracers position (Fig. 3h) shows that the plume head is strongly stretched and heterogeneous, and that a considerable fraction of tracers is trapped at the bottom. A detail of the forward calculation is shown in Fig. 3i. Material originally at distance less than 300 km (black and red tracers) can be
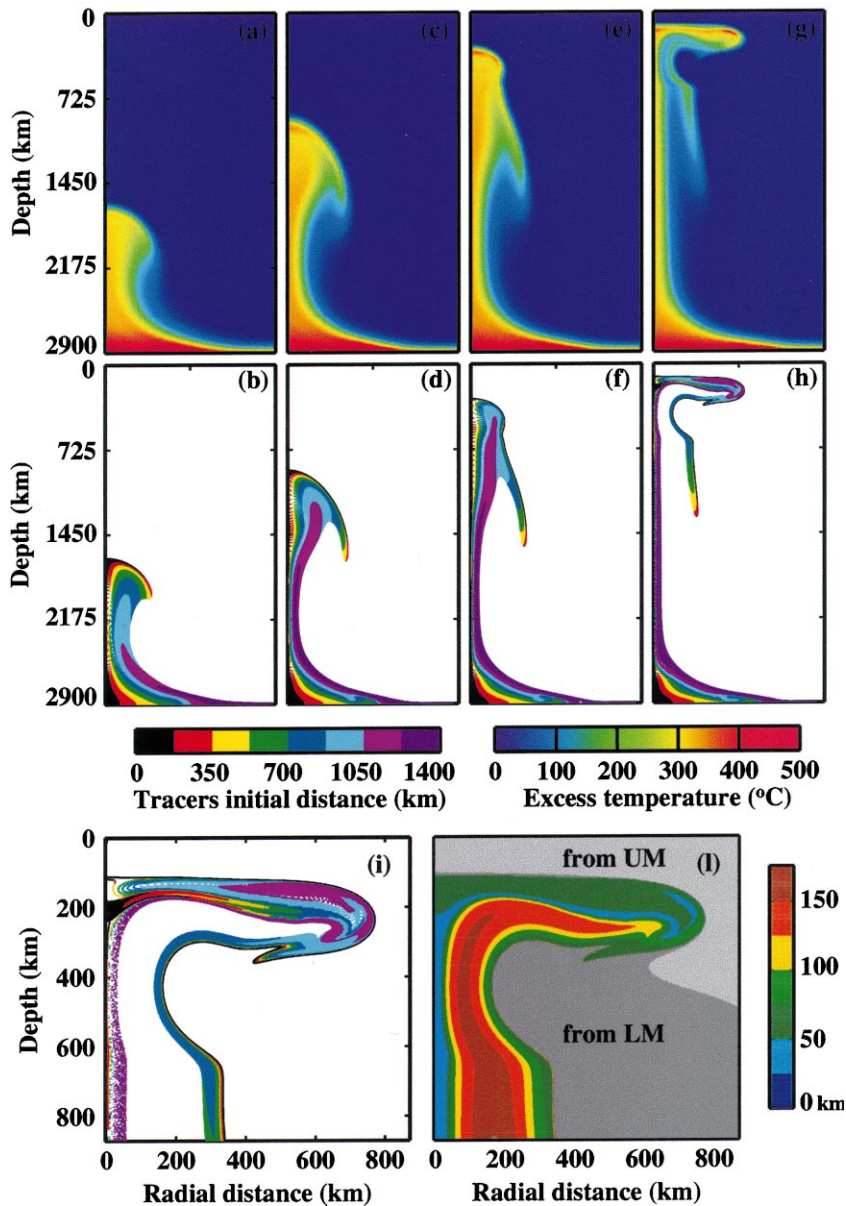
Fig. 3. Plume evolution for Model 3. Top: excess temperature. Middle: tracers advected forward. (i) Detail of the plume head shown in 3h. (l) Tracers advected backward.

found in the plume head both close to the axis, than stretched in a rim all around the head, also in this case the plume head is very heterogeneous. The results of the backward calculation (Fig. 3l) indicate that tracers from the lowermost 25 km are absent from the plume head, while material originally 150 km above the CMB occu-

pies the zone in the head with lowest excess temperatures.

3.2. Vertical displacements and deformations

The vertical displacement is shown in Fig. 4 for the three models. This figure is obtained by ad-

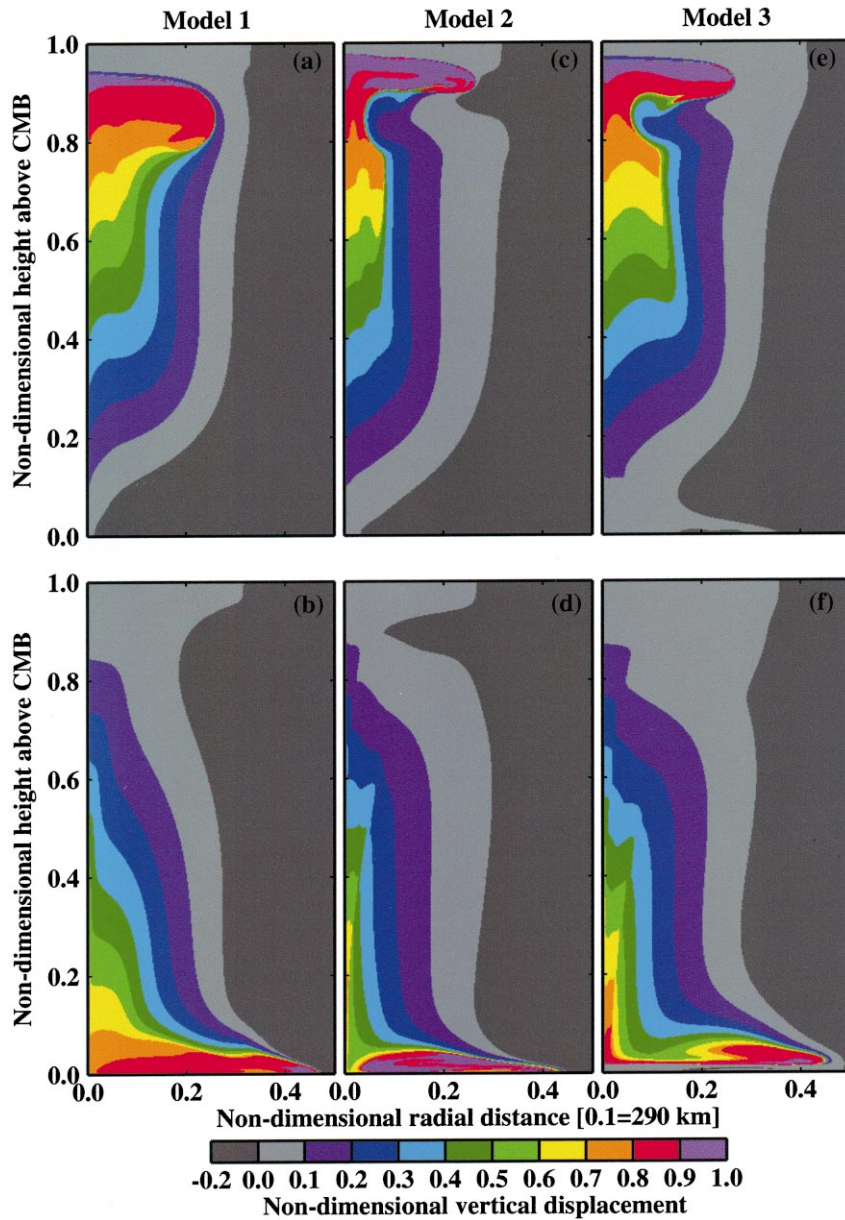Fig. 4. Vertical displacements over the interval $[t_0, t_1]$. Top: Plotted as a function of the final position, using backward advection. Bottom: Plotted as a function of the initial position, using forward advection. The color scale is the same for all panels.

vecting backward and forward in time 100 tracers in each grid element. For each model, the colored regions contain the same material at both the initial and the final time. The descending motion (in dark gray) occurs on the periphery of the domain to replace the material pumped into the plume.

Backward tracers advection (top panels) show that (i) the material with the highest vertical displacement is concentrated in the head, (ii) the interface with the surrounding material with low displacement is sharp on the top side of the head. Forward tracers advection (bottom panels) shows

that material at the base rises the most, except for a thin chemically denser layer in Model 3 (Fig. 4f). In all models there is a sharp transition in the thermal boundary layer between tracers with high vertical displacement and tracers with low (or negative) vertical displacement. Highest values along the axis are due to the efficient vertical displacement in the plume tail. The reverse vertical ordering of colors at the initial and final time is due to the penetration of the plume across the mantle with very little entrainment. The yellow and green regions consist of lower mantle material which rise significantly but it remains screened from the plume head by deeper material.

Fig. 5 shows the finite-time Lyapunov exponents, or finite-time deformation, plotted at the final and initial time (top and bottom panels, respectively). It is clear that the strongest deformation is highly localized. We recall that the deformation is the exponential of the Lyapunov exponent. For Model 1 (Fig. 5a) the most deformed region corresponds to the stretched rim of the plume head where tracers of different radial distance come in close contact. It is interesting to note that high values extend also in the portion of the upper mantle that has been displaced by the rising plume. In other words, the most deformed part in the upper mantle is the frontier between the head and the surrounding mantle in contact with it. The fact that maximum stretched regions are also dynamical barriers is often observed in chaotic geophysical flows [24–26]. At the initial time (Fig. 5b), the maximum stretched region is located in a sloping annular layer which is also marking the boundary between the ascending and the descending material in Fig. 4b. For Model 2 (Fig. 5c) the viscosity contrast between upper and lower mantle significantly increases the deformations. Once again the highest values correspond to the boundary of the plume head. Since a tongue is left behind in the lower mantle, and material is entrained between this tongue and the tail, the boundary is much more convoluted than for Model 1 and the whole head exhibits higher deformation. It is apparent that the maximum stretched layer divides the plume head in several subdomains originating from different reservoirs. The location of the maximum stretched region at

initial time (Fig. 5d) is also more convoluted and splitted in several parts corresponding again to the lines of sharp variation of the vertical displacement in Fig. 4d. The same features are shown in Fig. 5e,f for Model 3 with smaller values of the Lyapunov exponent since the elapsed time is much longer than in the other two cases, while the accumulated deformation, measured by σ_+, remains of the same order.

We find that for all models the deformations in the plume tail are weaker than in the leading plume head. We also find that the viscosity contrast between the upper and lower mantle has the most dramatic effect on the dynamics and on stirring, while the presence of the chemically denser layer in Model 3 reduces the plume ascent and enhances the entrainment of lower mantle by trapping the denser material in the foot of the plume.

3.3. Heterogeneities in the long-lived plume tail

The results presented above indicate that deformations in the plume tail may be lower than in the plume head. Here we investigate in more detail the dynamics of a long-lived plume tail, by carrying on the calculations for 80 Myr after the onset of partial melting.

The new model includes the mechanical effect of the endothermic phase transition at 660 km depth, with Clapeyron slope $\gamma = -3$ MPa/K. The density contrast induced by the phase transition is 8%, while the viscosity contrast between upper and lower mantle is one order of magnitude. In order to obtain plume excess temperatures around 250°C, comparable with values inferred from petrology, the initial excess temperature across the thermal boundary is now 350°C. The calculated buoyancy flux across the plume tail, at 250 km depth, is 7.3 Mg/s (after 20 Myr from the onset of melting), 4.9 Mg/s (after 40 Myr) and 4.4 Mg/s (after 80 Myr). For comparison, the estimated buoyancy flux for Hawaii is 8.7 Mg/s and for Iceland is 1.4 Mg/s [28], thus indicating that we are modeling a fairly strong and long-lived plume.

We advect packs of tracers randomly distributed in the lowermost mantle with an arbitrary initial size of 25×25 km, the total volume of
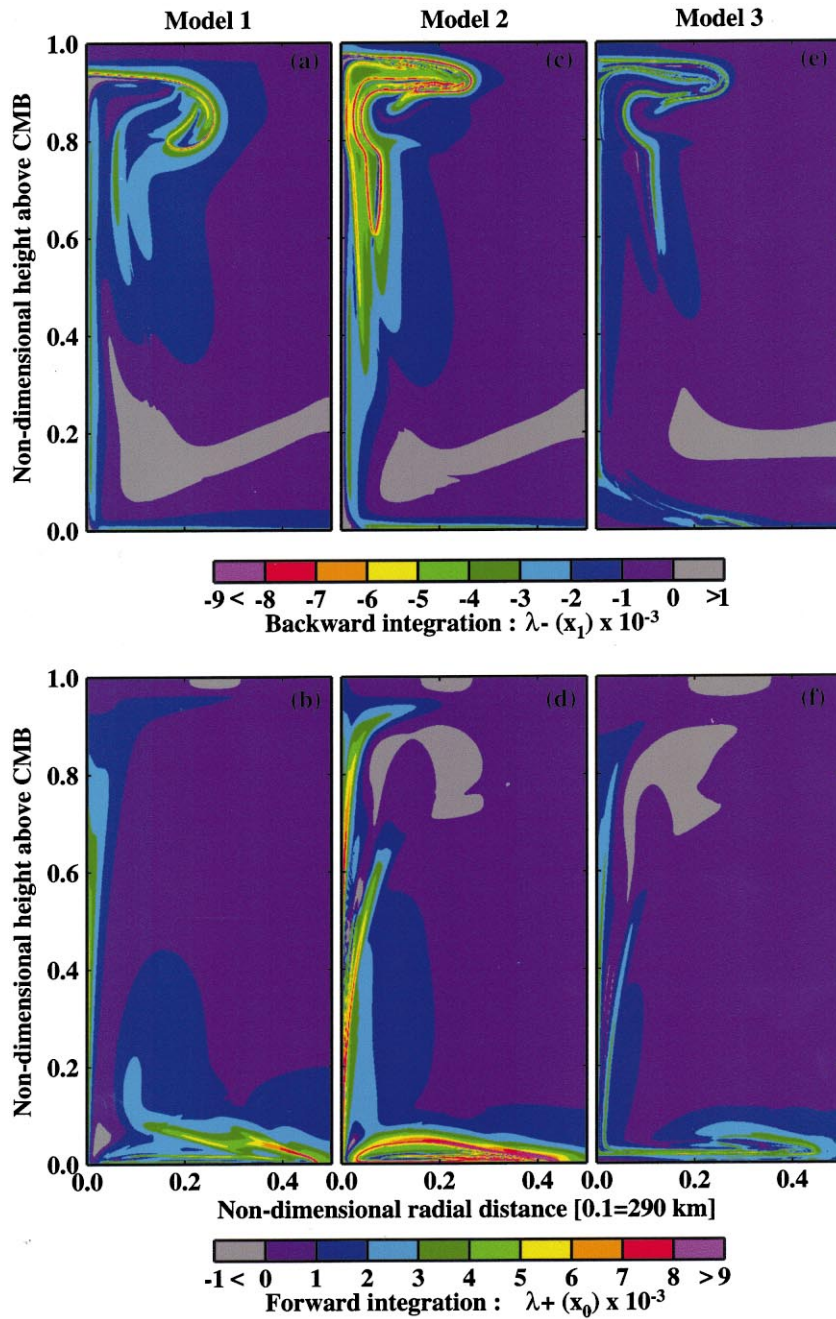
Fig. 5. Lyapunov exponents over the interval $[t_0, t_1]$. Top panels: $\lambda_-(x_1)$ for backward integration. Bottom panels: $\lambda_+(x_0)$ for forward integration.

this heterogeneous material represents 10% of the thermal boundary layer volume. Fig. 6 shows the plume head 40 Myr after the onset of melting. The heterogeneities are reduced to narrow fila-

ments in the plume head, while they are less deformed in the long-lived plume tail. Material from a 50-km thick zone just above the phase transition (gray color in Fig. 6) does not enter in the melting
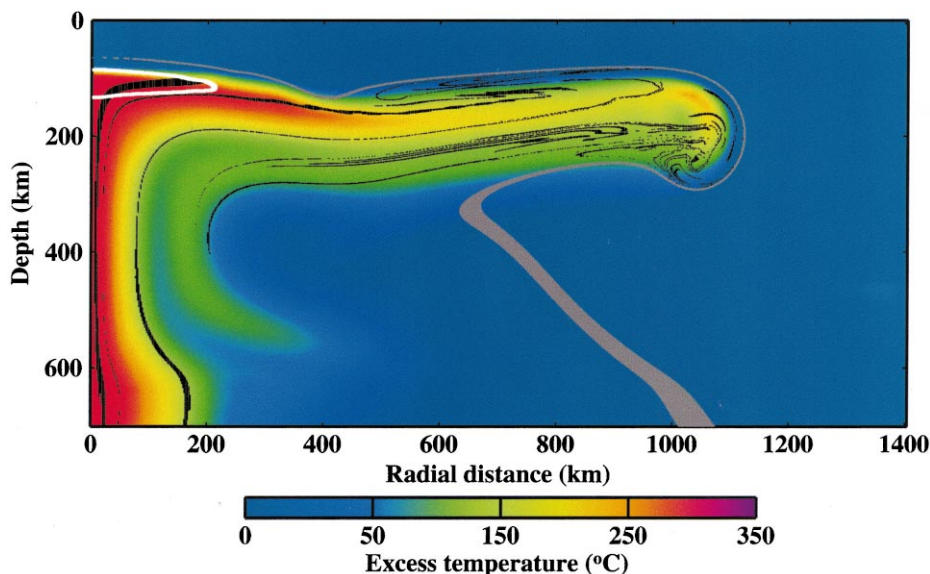
Fig. 6. Plume head 40 Myr after the onset of melting. Black tracers: stretched heterogeneities initially in the thermal boundary layer. Gray tracers: come from 660–620 km depth. The white contour surrounds the region of partial melting.

region but closely surrounds the plume head. Therefore, the phase transition does not represent a barrier to the ascending flow and entrainment of upper mantle material is not enhanced. However, the joint effect of a phase transition and of the viscosity contrast between upper and lower mantle induces the formation of a 'reservoir' of hot plume material ponding beneath the phase transition. Similar to Model 2 the plume head is fed by a secondary conduit parallel to the axial conduit. This complex structure may reduce the volume of material satisfying the pressure–temperature conditions required for partial melting. To investigate which fraction of plume material undergoes partial melting we advect thousand of tracers and at each time step we compare the real temperature of each tracer with the corresponding solidus temperature, given by the empirical formulation of Zhang and Herzberg [27] which best fits the melting data on anhydrous peridotite at pressures between 5 and 15 GPa: $T_s = 1002 - 0.96 P^2 - 465 \ln(1/P)$, where P is the lithostatic pressure. We find that only the axial part of the plume head partially melts, while the lower part of the plume head, fed by the tongue trapped in the lower mantle, never melts. (For sake of clearness the

position of all the tracers crossing the zone of partial melting is not shown in Fig. 6).

Although the melting model is very crude and the extent of the melting region depends on several parameters, including the thickness of the lithosphere, the pressure–temperature conditions and the fluid content, this result suggests that plumes efficiently inject deep heterogeneous material into the upper mantle and that just a fraction of it partially melts. Therefore, unmelted plume head material may 'pollute' the upper mantle and we speculate that it could be responsible for some of the geochemical diversity of MORBs.

4. Conclusions

We have used a numerical model to investigate mixing and deformations for plumes that originate from the thermal boundary layer at the base of the Earth's mantle, while we did not consider plumes that may ascend from the top of dome-like structures associated to large scale thermo-chemical convection [18,29]. Therefore we consider that our models are more appropriate for hotspots like Hawaii and Iceland, rather

than for the numerous hotspots of the South Pacific.

Our results indicate that

1. the thermal boundary layer, from which plumes originate, is the region most efficiently sampled. Therefore, we may speculate that the geochemically heterogeneous nature of mantle plumes is inherited at the source, rather than being entrained during the ascent. Since we do not model magma ascent we cannot investigate the role of lithospheric and crustal contamination on the geochemical signature of hotspot lavas.
2. Upper mantle material is not entrained, but it is displaced by the plume, thus we predict that present-day upper mantle, source of MORB, is not involved in the production of plume lavas. Therefore, we may speculate that the geochemically depleted component in vigorous plumes, such as Hawaii and Iceland, is due to the presence of subducted and recycled ancient depleted material. This is in good agreement with geochemical observations for Hawaii [4] and Iceland [2].
3. Material in the plume head is highly deformed and stirred by a series of stretching and folding events occurring during the plume rise. Heterogeneities initially present in the source region may be reduced to narrow filaments in the plume head. We also find that stirring and deformation in the plume tail are lower than in the plume head. Therefore, we may speculate that a same pack of subducted/recycled crust+lithosphere may still show a distinct geochemical signature in hotspot lavas, consistent with geochemical data [1].
4. By including a very crude melting model we find that only part of a plume head partially melts. This allows us to speculate that heterogeneous deep mantle material may be injected in the upper mantle and may give rise to geochemical heterogeneities when sampled by spreading ridges, even at great distance from the plume axis.
5. The phase transition at 660 km depth does not represent a barrier to vigorous ascending plume, in agreement with previous works

(e.g., [3]) and it does not have a profound effect on stirring and entrainment of upper mantle in the plume head. We find that material just above the transition zone (i.e., from 660 to 620 km depth) closely surrounds the plume head. Although in our simple model this 'sheath' of material does not melt, we cannot exclude that it may melt in case of decompressional melting induced by rifting, such as for Iceland.
6. The finite-time Lyapounv exponents, indicators of deformations, show that the boundary between the plume head and the upper mantle undergoes significant deformation. This could induce seismic anisotropy in the shallow upper mantle all around the large initial plume head. To our knowledge this testable hypothesis has not been investigated by seismologists.

Acknowledgements

References

[1] J.C. Lassiter, E.H. Hauri, Osmium-isotope variations in hawaiian lavas: evidence for recycled oceanic crust in the Hawaiian plume, Earth Planet. Sci. Lett. 164 (1998) 483–496.

[2] P.D. Kempton, J.G. Fitton, A.D. Saunders, G.M. Nowell, R.N. Taylor, B.S. Hardarson, G. Pearson, The Iceland plume in space and time: a Sr−Nd−Pb−Hf study of the North Atlantic rifted margin, Earth Planet. Sci. Lett. 177 (2000) 255–271.

[3] P.F. Thompson, P.J. Tackley, Generation of mega-plumes from the core-mantle boundary in a compressible mantle with temperature-dependent viscosity, Geophys. Res. Lett. 25 (1998) 1999–2002.

[4] E.H. Hauri, J.C. Lassiter, D.J. DePaolo, Osmium isotope systematics of drilled lavas from Mauna Loa, Hawaii, J. Geophys. Res. 101 (1996) 11793–11806.

[5] J. Blicher-Toft, F.A. Frey, F. Albarède, Hf isotope evidence for pelagic sediments in the source of hawaiian basalts, Science 285 (1999) 879–882.

[6] A.W. Hofmann, W.M. White, Mantle plumes from ancient oceanic crust, Earth Planet. Sci. Lett. 57 (1982) 421–436.

[7] M. Honda, I. McDougall, D.B. Patterson, A. Doulgeris, D.A. Clague, Noble gases in submarine pillow basalt glasses from Loihi and Kilauea, Hawaii: A solar component in the Earth, Geochim. Cosmochim. Acta 57 (1993) 859–874.

[8] E.T. Dixon, M. Honda, I. McDougall, I.H. Campbell, I. Sigurdsson, Preservation of near-solar neon isotopic ratios in Icelandic basalts, Earth Planet. Sci. Lett. 180 (2000) 309–324.

[9] M. Moreira, K. Breddam, J. Curtice, M.D. Kurz, Solar neon in the Icelandic mantle: new evidence for an undegassed lower mantle, Earth Planet. Sci. Lett. 185 (2001) 15–23.

[10] C. Mégnin, B. Romanowicz, The three-dimensional shear velocity structure of the mantle from the inversion of body, surface and higher-mode waveforms, Geophys. J. Int. 143 (2000) 709–728.

[11] C.J. Allègre, Limitation on the mass exchange between the upper and lower mantle: the evolving convection regime of the Earth, Earth Planet. Sci. Lett. 150 (1997) 1–6.

[12] A.V. Sobolev, A.W. Hofmann, I.K. Nikogosian, Recycled oceanic crust observed in 'ghost plagioclase' within the source of Mauna Loa lavas, Nature 404 (2000) 986–989.

[13] C.J. Allègre, D. Turcotte, Implications of a two component marble-cake mantle, Nature 323 (1986) 123–127.

[14] H. Samuel, C.G. Farnetani, Thermochemical convection and helium concentrations in mantle plumes, J. Geophys. Res. (2001) submitted.

[15] C.G. Farnetani, M.A. Richards, Thermal entrainment and melting in mantle plumes, Earth Planet. Sci. Lett. 136 (1995) 251–267.

[16] R.W. Griffiths, I.H. Campbell, Stirring and structure in mantle starting plumes, Earth Planet. Sci. Lett. 99 (1990) 66–78.

[17] A. Lenardic, W.M. Kaula, A numerical treatment of geodynamic viscous flow problems involving the advection of material interface, J. Geophys. Res. 98 (1993) 8243–8260.

[18] P.J. Tackley, Three-dimensional simulations of mantle convection with a thermo-chemical basal boundary layer: D″?, in: M. Gurnis, M.E. Wysession, E. Knittle, B.A. Buffett, (Eds.), The Core-mantle Boundary Region, AGU Geophys. Monogr. 28, 1998, pp. 231–253.

[19] Q. Williams, E.J. Garnero, Seismic evidence for partial melt at the base of the Earth's mantle, Science 273 (1996) 1528–1530.

[20] C.G. Farnetani, Excess temperature of mantle plumes: The role of chemical stratification across D″, Geophys. Res. Lett. 24 (1997) 1583–1586.

[21] H. Akima, Algorithm 760: rectangular-grid-data surface fitting that has the accuracy of a bicubic polynomial, ACM Trans. Math. Softw. 22 (1996) 357–361.

[22] J.M. Ottino, The kinematics of mixing: stretching, chaos and transport, Cambridge University Press, Cambridge, 1989.

[23] B. Legras, R. Vautard, A guide to Lyapunov vectors, in: T. Palmer (Ed.), Predictability, Semin. Proc. 1, European Center for Medium Range Weather Forecast, Reading, 1996, pp. 143–156.

[24] G. Lapeyre, P. Klein, B.L. Hua, Does the tracer gradient vector align with the strain eigenvectors in 2-D turbulence?, Phys. Fluids 11 (1999) 3729–3737.

[25] G. Haller, G. Yuan, Lagrangian coherent structures and mixing in two-dimensional turbulence, Phys. D 147 (2000) 352–370.

[26] B. Joseph, B. Legras, On the relation between kinematic boundaries, stirring, and barriers for the Antarctic polar vortex, J. Atmos. Sci. (2001), in press.

[27] J. Zhang, C. Herzberg, Melting experiments on anhydrous peridotite KLB-1 from 5.0 to 22.5 GPa, J. Geophys. Res. 99 (1994) 17727–17742.

[28] N.H. Sleep, Hotspots and mantle plumes: Some phenomenology, J. Geophys. Res. 95 (1990) 6715–6736.

[29] A. Davaille, Simultaneous generation of hotspots and superswells by convection in a heterogeneous planetary mantle, Nature 402 (1999) 756–760.